THE JOURNAL OF BIOLOGICAL CHEMISTRY VOL. 287, NO. 17, pp. 13930–13943, April 20, 2012

ATP Binding Site Mutagenesis Reveals Different Subunit Stoichiometry of Functional P2X2/3 and P2X2/6 Receptors*[S]

Received for publication, January 21, 2012, and in revised form, February 27, 2012 Published, JBC Papers in Press, February 29, 2012, DOI 10.1074/jbc.M112.345207

Ralf Hausmann[‡1], Mandy Bodnar[§1], Ronja Woltersdorf[‡], Haihong Wang[§], Martin Fuchs[§], Nanette Messemer[§], Ying Qin[§], Janka Günther[‡], Thomas Riedel[§], Marcus Grohmann[‡§], Karen Nieber[¶], Günther Schmalzing[‡], Patrizia Rubini[§2], and Peter Illes[§2,3]

From the [‡]Department of Molecular Pharmacology, University Hospital of Rheinisch Westfaelische Technische Hochschule, Aachen University, 52074 Aachen, Germany, the [§]Rudolf Boehm Institute of Pharmacology and Toxicology, University of Leipzig, Haertelstrasse 16-18, 04107 Leipzig, Germany, and the [¶]Department of Pharmacology for Natural Sciences, Institute of Pharmacy, University of Leipzig, 04103 Leipzig, Germany

Background: Heteromeric P2X receptors increase the diversity of rapid ATP signaling.
Results: Non-functional P2X2, P2X3, and P2X6 subunit mutants were used to investigate the composition of heteromeric P2X2/3 and P2X2/6 receptors.
Conclusion: The subunit stoichiometry of P2X2/3 and P2X2/6 is 1:2 and 2:1, respectively.
Significance: Recognition sites between P2X2 and its partners rather than random association may govern the subunit composition of the receptor trimers.

The aim of the present experiments was to clarify the subunit stoichiometry of P2X2/3 and P2X2/6 receptors, where the same subunit (P2X2) forms a receptor with two different partners (P2X3 or P2X6). For this purpose, four non-functional Ala mutants of the P2X2, P2X3, and P2X6 subunits were generated by replacing single, homologous amino acids particularly important for agonist binding. Co-expression of these mutants in HEK293 cells to yield the P2X2 WT/P2X3 mutant or P2X2 mutant/P2X3 WT receptors resulted in a selective blockade of agonist responses in the former combination only. In contrast, of the P2X2 WT/P2X6 mutant and P2X2 mutant/P2X6 WT receptors, only the latter combination failed to respond to agonists. The effects of α,β-methylene–ATP and 2-methylthio-ATP were determined by measuring transmembrane currents by the patch clamp technique and intracellular Ca^{2+} transients by the Ca^{2+}-imaging method. Protein labeling, purification, and PAGE confirmed the assembly and surface trafficking of the investigated WT and WT/mutant combinations in *Xenopus laevis* oocytes. In conclusion, both electrophysiological and biochemical investigations uniformly indicate that one subunit of P2X2 and two subunits of P2X3 form P2X2/3 heteromeric receptors, whereas two subunits of P2X2 and one subunit of P2X6 constitute P2X2/6 receptors. Further, it was shown that already two binding sites of the three possible ones are sufficient to allow these receptors to react with their agonists.

Cys-loop, pentameric (1–3), and tetrameric (4, 5) ligand-gated ion channels usually consist of the heteromeric composition of structurally divergent subunits. Homomeric assemblies of identical subunits are, however, to a minor extent also possible (*e.g.* for the $5HT_3$ receptor and certain neuronal nicotinic and $GABA_A$ receptor subtypes). More recently, an additional ATP-gated ionotropic receptor family has been discovered by cloning seven distinct P2X receptor subunits from mammalian species (P2X1 to -7) (6–9). Again, P2X subunits appeared to form not only homomeric receptor channels but also heteromeric ones. Original work based on co-immunoprecipitation with epitope-tagged subunits demonstrated that only P2X6 was not able to form homooligomers, and P2X7 was the only exception of constituting heterooligomeric complexes (10). Subsequently, it was found that P2X1/2 (11, 12), P2X1/4 (13), P2X1/5 (14), P2X2/3 (15), P2X2/6 (16), and P2X4/6 (17) receptors combine the original pharmacological and biophysical properties of their parent subunits. The huge diversity of native P2X receptors and their characteristics, often differing from those of the recombinant receptors, have been explained by the existence of heteromeric subunit compositions (18).

Despite these findings relating to recombinant receptors and the evidence that three subunits form both homomeric and heteromeric P2X receptors (6, 19, 20), two further points still need extensive clarification. First, only P2X2/3 (sensory ganglia) (21, 22), P2X1/5 (astrocytes) (23, 24), and probably P2X2/6 (neural stem cells) (25, 26) receptors were shown to occur under native conditions, whereas native P2X1/2, P2X1/4, and P2X4/6 receptors were hitherto not identified. Second, the subunit stoichiometry of functional P2X2/3 receptors appears to be 1:2 (27, 28), but for the residual heteromeric receptors, there are no comparable data available.

In the case of the P2X2/3 receptor, two homologous amino acid (AA)[4] residues participating in agonist binding were

* This work was supported by Deutsche Forschungsgemeinschaft Grant FOR 748 and the Volkswagen Foundation.
[S] This article contains supplemental Figs. 1 and 2.
[1] Both authors contributed equally to this work.
[2] Both authors contributed equally to this work.
[3] To whom correspondence should be addressed. Tel.: 49-341-9724614; Fax: 49-341-9724609; E-mail: Peter.Illes@medizin.uni-leipzig.de.

[4] The abbreviations used are: AA, amino acid; NBS, nucleotide binding segment; hP2X2, hP2X3, and hP2X6, human P2X2, P2X3, and P2X6, respectively; 2-MeSATP, 2-methylthio-ATP; α,β-meATP, α,β-methylene–ATP; BN, blue native.

replaced individually with alanine to yield inactive mutants of P2X2 and P2X3 subunits; combination of the mutant P2X3 with wild-type (WT) P2X2 resulted in a non-functional receptor, whereas the opposite combination was fully active (28). Unfortunately, there were no accompanying biochemical data presented to confirm that the functionally silent AA mutants of P2X2 and P2X3 and their compositions with their WT counterparts still exhibited undisturbed trafficking behavior and were expressed at the cell surface.

In P2X receptors, instead of a few AA residues, four clusters of AAs, termed nucleotide binding domains (NBD1 to -4) (29) (here nucleotide binding segments, NBS1 to -4), were identified as possible docking places for ATP. NBS1 and -2 appear to be located at one subunit, whereas NBS3 and -4 are situated at the neighboring subunit (30) in accordance with the recently described crystal structure of the zebrafish P2X4 receptor (31).

The aim of the present experiments was to find out whether two heteromeric receptors (P2X2/3 and P2X2/6), where P2X2 combines with two different partners, have an obligatory subunit stoichiometry of 1:2 or whether the subunit stoichiometry may be variable. For this purpose, we used the ATP structural analogues 2-methylthio-ATP (2-MeSATP) and α,β-methylene–ATP (α,β-meATP) as well as non-functional mutants of P2X2 and P2X3 with a single Ala mutation in NBS1 to -4 each. Moreover, we also used homologous mutants of P2X6 to clarify the subunit stoichiometry of the P2X2/6 receptor. Electrophysiological measurements and Ca^{2+} imaging as well as protein labeling, purification, and PAGE suggested that P2X2/6 receptors consist of two P2X2 subunits and one P2X6 subunit and thereby differ from P2X2/3 receptors.

EXPERIMENTAL PROCEDURES

Culturing of HEK293 Cells—HEK293 cells were kept in Dulbecco's modified Eagle's medium also containing 4.5 mg/ml D-glucose (Invitrogen), 2 mM K-glutamine (Sigma-Aldrich), 10% fetal bovine serum (Invitrogen) at 37 °C and 10% CO_2 in humidified air.

Site-directed Mutagenesis and Transfection Procedures—The human P2X2 ($hP2X2_A$), hP2X3 (gift of J. N. Wood, University College, London, UK), and hP2X6 (gift of A. Surprenant, University of Manchester, Manchester, UK) cDNAs were subcloned at PstI and EcoRI restriction sites into pIRES2-EGFP (P2X3 and P2X6) or pIRES2-Ds-Red (P2X2) vectors from Clontech for independent expression of the respective P2X subunit and EGFP or Ds-Red, creating the pIR-P2X plasmid. All P2X subunit mutants were generated by introducing replacement mutations into the pIR-P2X construct using the QuikChange site-directed mutagenesis protocol from Stratagene according to the instruction manual. HEK293 cells were plated in plastic dishes (electrophysiology) or onto coverslips (Ca^{2+} imaging) 1 day before transient transfection. 0.5 μg of plasmid DNA (homomeric P2X2, P2X3, and P2X6 receptors; heteromeric P2X2/3 and P2X2/6 receptors, 1:2 ratio) or 0.75 μg of plasmid DNA (P2X2/6 receptors, 1:4 ratio) was combined with 10 μl of PolyFect reagent from Qiagen and 100 μl of Opti-MEM (Invitrogen).

Whole-cell Patch Clamp Recordings—Whole-cell patch clamp recordings were made after transient transfection of HEK293 cells, at room temperature (20–22 °C), using an Axopatch 200B patch clamp amplifier (Molecular Devices) as described previously (30). Transfected HEK293 cells were searched for by means of a reverse differential interference contrast microscope with epifluorescent optics (Axiovert 100, Zeiss). The pipette solution contained 140 mM CsCl, 1 mM $CaCl_2$, 2 mM $MgCl_2$, 10 mM HEPES, and 11 mM EGTA, pH adjusted to 7.3 using CsOH. When 2-MeSATP was used as an agonist, GDP-β-S (300 μM) was also included, in order to eliminate the negative interaction between P2Y and P2X receptors in HEK293 cells (31). The external physiological solution contained 135 mM NaCl, 4.5 mM KCl, 2 mM $CaCl_2$, 2 mM $MgCl_2$, 10 mM HEPES, and 10 mM glucose, pH adjusted to 7.4 using NaOH. The pipette resistances were 3–6 megaohms. Holding potential values were corrected for the calculated liquid junction potential between the bath and pipette solution. All recordings were made at a holding potential of −65 mV. Data were filtered at 2 kHz with the built-in filter of the amplifier, digitized at 5 kHz, and stored on a laboratory computer using a Digidata 1440 interface and pClamp 10.2 software (Molecular Devices).

Drugs were dissolved in the external solution and locally superfused over single cells (detected by their EGFP and/or DS-Red fluorescence), using a rapid solution change system (SF-77B Perfusion Fast Step, Warner Instruments). Concentration-response curves were established by applying increasing concentrations of α,β-meATP or 2-MeSATP (both from Sigma-Aldrich) for 2 s. The intervals between applications were kept at 5 min throughout. Under these conditions, agonist responses were reproducible, with the exception of those to 2-MeSATP at HEK293-P2X3 cells; the marked desensitization at higher concentrations of 2-MeSATP (>3 μM) was in accordance with the reported long period of time required to regain 50% of control peak amplitude when determined with a paired-pulse protocol (32) (see also supplemental Fig. 1*Ac*, *right*).

The desensitization time constants (τ_{des1} and τ_{des2}) and the recovery of P2X3 receptors from desensitization were determined as described previously (supplemental Fig. 1*Ac*, *left*) (33). For the measurement of the recovery from desensitization, HEK293 cells were stimulated repetitively with α,β-meATP (30 μM; 2-s pulses) with a progressive increase in the interpulse intervals. We measured the t_{50} value, which is the time needed to regain 50% of maximally recovered currents. Only the τ_{des1} values are indicated, because the rapid phase of desensitization appears to be the more relevant one.

Ca^{2+} Microfluorometry—HEK293 cells were loaded 2–3 days after transient transfection, with the Ca^{2+}-sensitive fluorescent dye Fura-2 acetoxymethyl ester (2.5 μM; Sigma-Aldrich) at 37 °C for 1 h in culture medium. Cells plated onto coverslips were mounted into the superfusion chamber and placed on the stage of an inverted microscope (IX-70; Olympus) with epifluorescent optics and a cooled CCD camera (IMAGO; Till Photonics). Throughout the experiments, cells were continuously superfused at 0.8 ml/min by means of a roller pump with external solution. Intracellular Fura-2 was alternately excited at 340 and 380 nm, and the emitted light was measured at a wavelength of 510 nm. The Till Vision software (version 3.3, Till Photonics) was used for data acquisition, system control,

and, later, off-line analysis. The fluorescence ratio (340/380 nm) provides a relative measure of the cytosolic free Ca^{2+} concentration ($[Ca^{2+}]_i$).

For the determination of concentration-response relationships, α,β-meATP or 2-MeSATP was pressure-injected locally, by means of a computer-controlled DAD12 superfusion system (ALA Scientific Instruments, Inc.). The application time was 5 s, and the intervals between two subsequent agonist applications were kept, independent of the concentration used, at 15 min. α,β-meATP is a selective P2X1, P2X3, P2X1/2, P2X1/5, and P2X2/3 receptor agonist (34), which does not activate endogenous P2Y receptors of HEK 293 cells (35). In contrast, 2-MeSATP is a non-selective P2X/Y receptor agonist (34, 36), which may cause an increase of $[Ca^{2+}]_i$ through the activation of G_q protein-coupled $P2Y_1$ receptors (35). In order to account for this problem, concentration-response curves for 2-MeSATP were constructed at HEK293 cells transfected with P2X2 subunits, P2X6 subunits, or their mutants as well as on mock-transfected cells. $[Ca^{2+}]_i$ responses caused by 2-MeSATP after mock transfection were subtracted from those obtained after transfection with the respective subunit plasmids (Fig. 3*Cb*) and yielded the $[Ca^{2+}]_i$ transients due to receptor stimulation only.

Expression of P2X2, P2X3, and P2X6 Receptors and Their Mutants in Xenopus laevis Oocytes—Oocyte expression plasmids harboring the cDNAs for N-terminally hexahistidine-tagged (His-tagged) $hP2X2_A$, hP2X3, or hP2X6 subunit have been described previously (12, 30). Replacement mutations or a StrepII affinity tag-encoding sequence 5′ of the stop codon were introduced by QuikChange site-directed mutagenesis (Stratagene). Capped cRNAs were synthesized and injected in aliquots of 46 nl into collagenase-defolliculated *X. laevis* oocytes using a Nanoliter 2000 injector (World Precision Instruments) as described previously (37). For expression of the heteromeric P2X2/3 receptor, cRNAs for the P2X2 and P2X3 subunit were co-injected at a 1:2 ratio (w/w). For expression of the heteromeric P2X2/6 receptor, the cRNAs for the P2X2 and P2X6 subunit were co-injected at a 1:4 ratio (w/w). Oocytes were cultured at 19 °C in sterile oocyte Ringer's solution (90 mM NaCl, 1 mM KCl, 1 mM $CaCl_2$, 1 mM $MgCl_2$, and 10 mM HEPES, pH 7.4) supplemented with 50 μg/ml gentamycin.

Two-electrode Voltage Clamp Electrophysiology—1–2 days after cRNA injection, current responses were evoked by 2-MeSATP (P2X2 and P2X2/6 receptors) or α,β-meATP (P2X2/3 receptors) as indicated at ambient temperature (21–24 °C), and recorded by conventional two-electrode voltage clamp with a Turbo TEC-05 amplifier (npi Electronics) at a holding potential of −60 mV as described previously (37). For concentration-response analysis, P2X receptor-mediated currents were induced in 60-s intervals by 10-s applications of increasing concentrations of the indicated agonist.

Protein Labeling, Purification, and PAGE— cRNA-injected oocytes were metabolically labeled by overnight incubation with L-[^{35}S]methionine (PerkinElmer Life Sciences) and, just before protein extraction, surface-labeled with the membrane-impermeable fluorescent dye Cy5 NHS ester (GE Healthcare) as described previously (38). Affinity-tagged proteins were purified by non-denaturing Ni^{2+}-NTA chromatography (Qiagen) or Strep-Tactin chromatography (IBA Germany) from digitonin (1%, w/v) extracts of oocytes as indicated. The P2X receptors were released in the non-denatured state from the Ni^{2+}-NTA-Sepharose or the Strep-Tactin-Sepharose with elution buffer consisting of 1% (w/v) digitonin in 250 mM imidazole/HCl (pH 7.6) or 1% (w/v) digitonin in 0.1 M sodium phosphate buffer, pH 8.0, supplemented with 10 mM biotin, respectively. Native proteins were analyzed by blue native PAGE (BN-PAGE) as described previously (12, 39). Where indicated, samples were treated before BN-PAGE for 1 h at 37 °C with 0.1% (w/v) SDS to induce partial dissociation of P2X receptor complexes. To avoid quenching of the fluorescence by the Coomassie G250 dye, BN-polyacrylamide gels were destained prior to fluorescence imaging by repeated cycles of incubation in 50% (v/v) acetonitrile (Biosolve) supplemented with 25 mM ammonium carbonate as described previously (40). The destained polyacrylamide gel was repeatedly washed in 0.1 M sodium phosphate buffer, pH 8.0, and scanned wet by a Typhoon 9410 scanner (GE Healthcare) for fluorescence detection. For the subsequent visualization of the ^{35}S-labeled proteins, the BN-polyacrylamide gels were dried, exposed to a phosphor screen, and scanned by a PhosphorImager (Storm 820, GE Healthcare).

For reducing SDS-PAGE, proteins were denatured by incubation with SDS sample buffer containing 20 mM DTT for 15 min at 56 °C and electrophoresed in parallel with ^{14}C-labeled molecular mass markers (Rainbow, Amersham Biosciences) on SDS-polyacrylamide gels (10% acrylamide). SDS-polyacrylamide gels were scanned wet with a fluorescence scanner (Typhoon 9410, GE Healthcare) for visualization of Cy5-labeled plasma membrane-bound proteins, and then we dried the gels for the subsequent detection of ^{35}S incorporation as described above.

The intensity of the fluorescent protein bands was quantified using the ImageQuant TL software version 7.0 (GE Healthcare). Images of polyacrylamide gels were prepared with ImageQuant TL for contrast adjustments. For better visibility of weak and strong protein bands, individual lanes from the same, but differently enhanced, ImageQuant image were cropped and positioned using Adobe Photoshop CS4. Microsoft PowerPoint 2003 was used for labeling. Each experiment was performed at least twice with equivalent results.

Homology Modeling—We modeled, based on the published crystal structure of the zebrafish P2X4 channel in its closed state (31), the extracellular loop and transmembrane areas of the hP2X2, hP2X3, and hP2X6 receptors. The software used was Modeler 9, version 7 (41). The alignment was determined by the align2D function, which also takes the secondary structure of the template into consideration. Homology modeling was made with the loop model function with high optimization settings. Visualization of the results was by VMD (42).

Data Analysis—Concentration-response curves for agonists were fitted by using a three-parametric Hill plot (SigmaPlot; SPSS). The figures show mean ± S.E. values of *n* experiments. One-way analysis of variance followed by the Holm-Sidak post hoc test was used for multiple comparisons with a control group or multiple pairwise comparisons. The differences between two groups were evaluated by the normality test followed by the Student's *t* test or the rank sum test, as appropri-

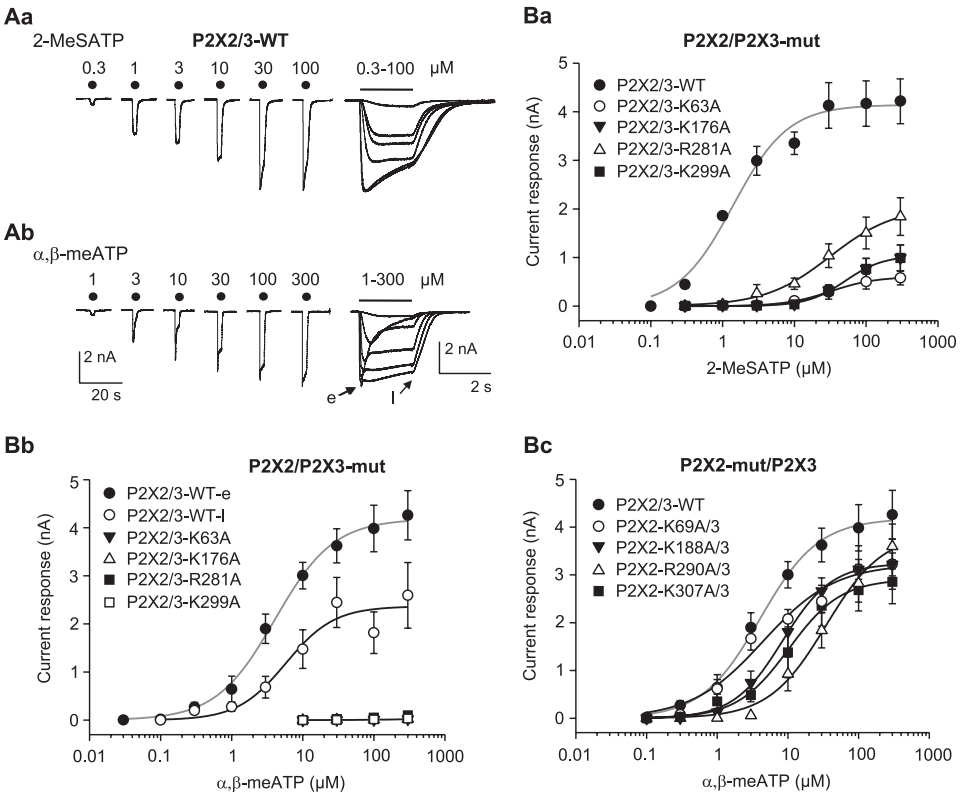

FIGURE 1. **Current responses at wild-type (*WT*) hP2X2/3 receptors and at the combinations of mutant (*mut*) hP2X2 or hP2X3 subunits with their WT partners expressed in HEK293 cells.** *A*, whole-cell currents induced by 2-MeSATP (*Aa*) or α,β-meATP (*Ab;* 0.3–100 μM) were recorded with the patch clamp technique at a holding potential of −65 mV. Increasing concentrations of the two agonists were locally superfused for 2 s with 5-min intervals (as indicated by *filled circles* or a *horizontal bar*), and the resulting currents were reproduced at two different time scales (note the divergent *calibration bars* on the *right* and *left*). α,β-meATP caused a rapidly desensitizing early current (*e*), followed by a more constant late current (*l*). *B*, concentration-response relationships constructed for 2-MeSATP (*Ba*) and α,β-meATP (*Bb* and *Bc*) at WT P2X2/3 receptors and their non-functional mutants, whose selected Lys and Arg residues were replaced by Ala. The concentration-response relationships at the WT homomeric or heteromeric receptor are shown in *gray*. Means ± S.E. (*error bars*) of 5–8 experiments are shown. The Hill coefficients for the respective concentration-response curves at WT P2X2/3 receptors were as follows: 1.1 ± 0.2 (2-MeSATP); 1.1 ± 0.1 (α,β-meATP, early), 1.3 ± 0.5 (α,β-meATP, late). The E_{max} and EC_{50} values for the late α,β-meATP concentration-response curves at WT P2X2/3 receptors were 2,365 ± 241 pA and 5.7 ± 2.2 μM. For all further E_{max} and EC_{50} values as well as the exact number of experiments, see Table 1.

ate. A probability level of 0.05 or less was considered to reflect a statistically significant difference.

RESULTS

Patch Clamp Investigations in HEK293 Cells—Alanine-scanning mutagenesis in the four NBSs in hP2X3 showed that the conserved K63A, K176A, R281A, and K299A mutants did not react with α,β-meATP (300 μM) at all or responded with very small current amplitudes only (30). The inactivity of the homologous Ala or Cys mutants in P2X1, P2X2, and P2X4 with ATP as an agonist was demonstrated previously (see Refs. 19, 43, and 44).

Both α,β-meATP and 2-MeSATP (0.3–100 μM each) caused fast inward currents at the holding potential of −65 mV (supplemental Fig. 1, *Aa* and *Ab*). The current responses desensitized already during the 2-s application period with a rapid onset, which was similar both for α,β-meATP and 2-MeSATP (30 μM each) (supplemental Fig. 1*Ac*, *left*). However, the recovery from desensitization, which probably reflects the dissociation of the agonist from the receptor, was much slower for 2-MeSATP than for α,β-meATP (30 μM each) (supplemental Fig. 1*Ac*, *right*; $p < 0.05$). In accordance with this observation, the E_{max} value of the concentration-response curve for 2-MeSATP was smaller than that of α,β-meATP (supplemental Fig. 1*B*; $p <$ 0.05). At the same time, the EC_{50} values of the two agonists also differed. In addition, we investigated the effect of 2-MeSATP (10–300 μM) at the mutant K176A and found that neither this agonist nor α,β-meATP (10–300 μM) caused any current response. Thus, K176A-hP2X3 was an inactive mutant irrespective of the type of agonist used.

In the following experiments, HEK293 cells transfected with WT or mutant P2X2 plus P2X3 cDNA plasmids, in a ratio of 1:2, were superfused with 2-MeSATP (0.1–300 μM) or α,β-meATP (0.03–300 μM) for 2 s every 5 min (Fig. 1, *A* and *B*). Although the E_{max} values and Hill coefficients of the concentration-response curves were comparable, the EC_{50} values of the two agonists differed from each other (Fig. 1, *A* and *B*, and Table 1; the peaks of the agonist-induced currents were evaluated at this stage). By keeping a 5-min interval between the applications of increasing 2-MeSATP concentrations, there was little desensitization within the 2-s application time (Fig. 1*Aa*). By contrast, with the same application protocol, α,β-meATP caused a rapid peak followed by a quasi-steady-state response (at the end of the 2-s superfusion period; Fig. 1*Ab*). Accordingly, a plot of the early peak response against the logarithmic α,β-meATP concentration resulted in a maximum of the curve (Table 1), which was higher than that obtained by plotting the late, quasi-steady-state current against the loga-

TABLE 1

Agonist sensitivities of P2X2, P2X3, P2X6, P2X2/3, and P2X2/6 receptors as well as of the combinations of the respective WT and mutant subunits expressed in HEK293 cells

Concentration-response curves for α,β-meATP or 2-MeSATP were determined by the whole-cell patch clamp method.

Receptor	Agonist	E_{max}	EC_{50}	*n*
		pA	μM	
P2X2 WT	α,β-meATP		>300	6
P2X3 WT		4,891 ± 85	2.1 ± 0.1	7
P2X3-K176A			>300	6
P2X2/3 WT		4,182 ± 93[a]	4.1 ± 0.4	8
P2X2/3-K63A			>300	6
P2X2/3-K176A			>300	6
P2X2/3-R281A			>300	6
P2X2/3-K299A			>300	6
P2X2-K69A/3		3,231 ± 240[b]	4.5 ± 1.4	6
P2X2-K188A/3		3,245 ± 45[b]	8,4 ± 0.4	7
P2X2-R290A/3		3,870 ± 266	34.3 ± 6.8[b]	7
P2X2-K307A/3		2,911 ± 101[b]	10.3 ± 1.2	7
P2X3 WT	2-MeSATP	1,811 ± 131[a]	0.9 ± 0.3	7
P2X3-K176A			>300	6
P2X2 WT		6,448 ± 29[a]	14.4 ± 0.2[a]	10
P2X2-K69A			>300	6
P2X2-K188A			>300	6
P2X2-R290A			>300	6
P2X2-K307A			>300	7
P2X2/3 WT		4,140 ± 139[a]	1.4 ± 0.2[c]	6
P2X2/3-K63A		607 ± 10[b]	31.7 ± 1.4[b]	7
P2X2/3-K176A		1,042 ± 32[b]	51.5 ± 3.5[b]	8
P2X2/3-R281A		2,044 ± 123[b]	31.6 ± 5.9[b]	6
P2X2/3-K299A		1,042 ± 32[b]	51.5 ± 3.5[b]	6
P2X6 WT			>300	7
P2X2/6 WT		3,202 ± 145[a]	30.5 ± 3.8	10
P2X2/6-K68A		3,385 ± 144	26.5 ± 3.2	6
P2X2/6-K191A		3,092 ± 93	24.3 ± 2.0	8
P2X2/6-R287A		4,488 ± 98[b]	18.2 ± 1.1[b]	6
P2X2/6-K305A		4,946 ± 131[b]	14.6 ± 1.2[b]	7
P2X2-K69A/6			>300	6
P2X2-K188A/6			>300	6
P2X2-R290A/6			>300	6
P2X2-K307A/6			>300	6

[a] $p < 0.05$; statistically significant difference from the respective values at the WT P2X3 receptor (P2X3 WT).
[b] $p < 0.05$; statistically significant difference from the respective values at the WT receptor.
[c] $p < 0.05$; statistically significant difference from the respective EC_{50} value at the P2X3 WT receptor with α,β-meATP as the agonist.

rithmic α,β-meATP concentration (Fig. 1*Bb*). However, the EC_{50} values of the "early" (Table 1) and "late" curves (Fig. 1*Bb*; $p > 0.05$) were similar. Thus, under our experimental conditions, a mixed P2X3-P2X2/3 initial response with a rapidly desensitizing P2X3 component was followed by a slowly desensitizing P2X2/3 component. It is noteworthy that the P2X2/3 currents could be investigated in isolation, when the receptor mutants were expressed in *X. laevis* oocytes (no early peak current because of strong residual desensitization at a drug-free interval of 1 min; supplemental Fig. 2*Aa*).

Then we demonstrated that although 2-MeSATP and α,β-meATP equally well activated the WT P2X2/3 receptor, 2-MeSATP still slightly stimulated the P2X2/3 heteromeric receptors containing WT P2X2 and mutant P2X3 (K63A, K176A, R281A, and K299A), whereas α,β-meATP had no effect at all at these complexes (Fig. 1, compare *Ba* and *Bb*, and Table 1). By contrast, when WT P2X3 was co-transfected together with the non-functional P2X2 mutants (K69A, K188A, R290A, and K307A) (Fig. 1*Bc*, and Table 1), at positions homologous to those targeted in the P2X3 mutants, the E_{max} values of α,β-meATP at all heteromeric receptors only slightly decreased, and all EC_{50} values with the exception of P2X2-R290A/P2X3 did not change (Fig. 1*Bc* and Table 1). Thus, heteromeric P2X2/3 receptors lost their original sensitivity toward agonists (α,β-meATP) or became much less sensitive (2-MeSATP) when the P2X3 subunits carried inactivating mutations but were only slightly affected when the P2X2 subunits carried the homologous mutations. These results can be explained by the assumption that one P2X2 subunit associates with two P2X3 subunits to form a P2X2/3 heteromer.

The following experiments were designed to clarify the subunit stoichiometry of P2X2/6 receptors. First of all, we transfected HEK293 cells with P2X6 subunits only and did not obtain any current response to 2-MeSATP (0.3–300 μM; Fig. 2*Aa*). Subsequently, transfections were made by P2X2 and P2X6 in combinations of 1:2 and 1:4. The WT P2X2/6 receptors at the 1:2 and 1:4 transfection ratios exhibited decreasing sensitivities to 2-MeSATP; the respective E_{max} values gradually decreased from the WT P2X2 to P2X2/6 (Fig. 2*Aa*; $p < 0.05$ each).

The slope of the current responses measured during the last 1 s of agonist application (out of the total 2-s duration) also differed between P2X2 and P2X2/6 ($p < 0.05$) (*e.g.* at 30 μM 2-MeSATP (*inset* to Fig. 2*Ab*; compare also the *right panels* of Fig. 2, *Ca* and *Cb*). At 2-MeSATP concentrations higher than 3 μM, there was an increasingly positive slope for the P2X2 curve up to a concentration of 100 μM, whereas the slope for the P2X2/6 (1:4 transfection ratio) curve was negative in this range of concentrations. The P2X2/6 (1:2 transfection ratio) curve was found to lie between the two other ones.

Gradual acidification of the bath solution from pH 7.4 to 5.4 only slightly increased the amplitudes of the 2-MeSATP (30 μM)-induced P2X2 but not P2X2/6 (1:2 transfection ratio; $p > 0.05$) currents, whereas there was a marked potentiation of the P2X2/6 (1:4 transfection ratio; $p < 0.05$) current amplitudes (Fig. 2, *Ba–Bc*). The sudden increase in amplitude with acidification observed with the transfection ratio 1:4, in contrast to the transfection ratio 1:2, may indicate that an excess of P2X6 over P2X2 is needed to generate a sufficient amount of P2X2/6 in the plasma membrane. Thus, all three experimental approaches prove that co-transfection with P2X2 and P2X6 subunits resulted in a presumably heteromeric receptor with functional properties differing from P2X2 only if the plasmid cDNA ratios amounted to 1:4. Therefore, this transfection procedure was used for all subsequent investigations.

Fig. 2, *Ca* and *Cb*, shows individual concentration response relationships for 2-MeSATP (1–300 μM) at homomeric P2X2 and heteromeric P2X2/6 receptors. As previously mentioned, the Ala replacement of four conserved AA residues in P2X2 at positions homologous to those targeted in P2X3 produced non-functional P2X2 receptors (Fig. 2*D* and Table 1). When WT P2X2 was used together with P2X6 mutants (K68A, K191A, R287A, and K305A) for co-transfecting HEK293 cells, the E_{max} and EC_{50} values indicated higher activity for the P2X2/P2X6-R287A and -K305A mutants, when compared with the WT P2X2/6 receptor, but not for the P2X2/P2X6-K68A and -K191A mutants (Fig. 2*Ea* and Table 1). In contrast, the non-functional P2X2 mutant components abolished the 2-MeATP effects at the respective P2X2/6 receptors. The results can be explained by the assumption that two P2X2 subunits associate with one P2X6 subunit to form a P2X2/6 heteromer (see also

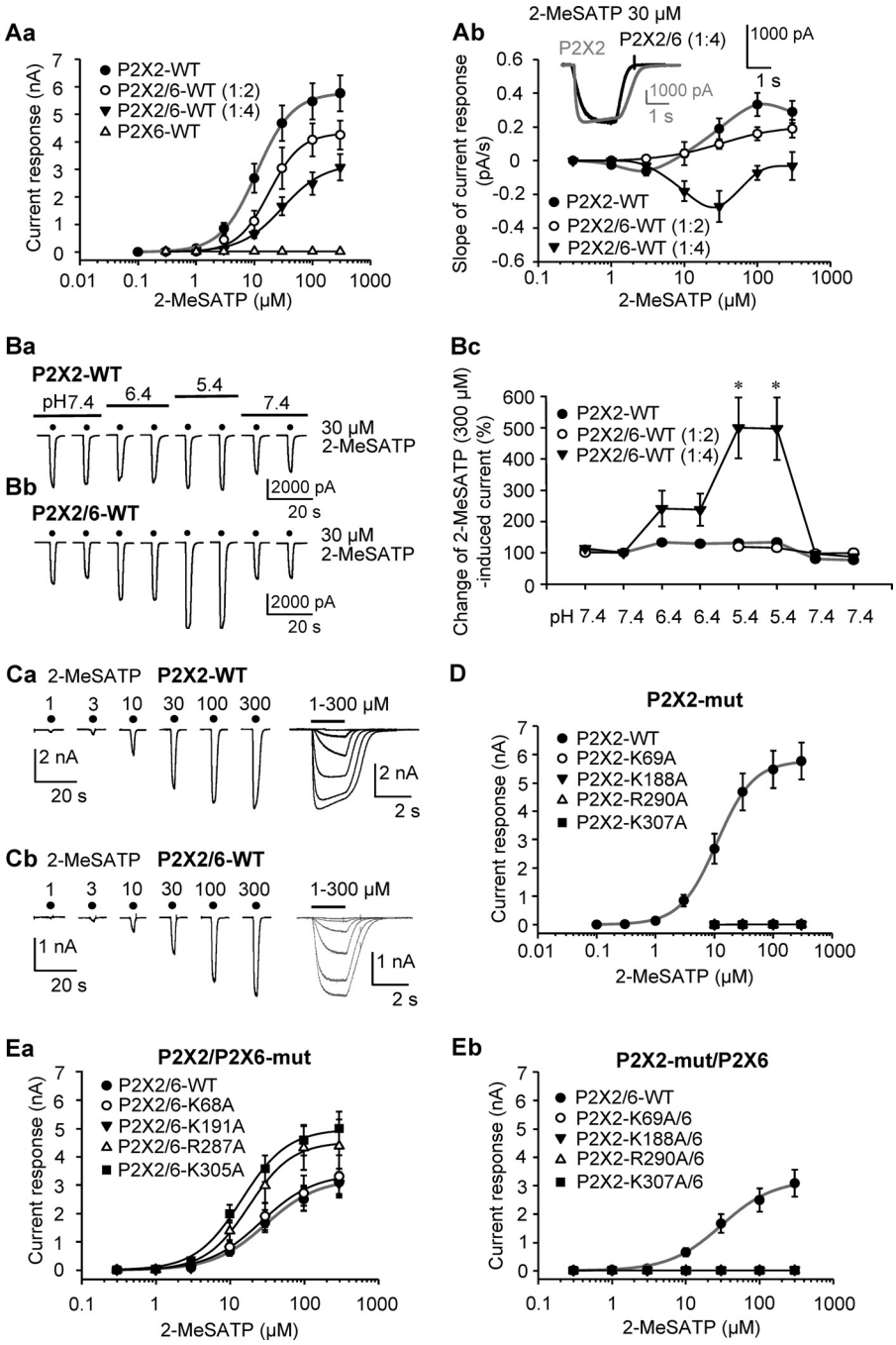

FIGURE 2. **Current responses at WT hP2X2, hP2X6, and hP2X2/6 receptors and at the combinations of the respective WT and mutant subunits expressed in HEK293 cells.** *A*, whole-cell currents at P2X2 or P2X2/6 (transfection ratios 1:2 or 1:4) receptors induced by 2-MeSATP (0.1–300 μM) were recorded with the patch clamp technique at a holding potential of −65 mV. Increasing concentrations of the two agonists were locally superfused for 2 s with 5-min intervals (for representative recordings and application protocol, see *C*). Shown are concentration-response relationships for the amplitude of the 2-MeSATP-induced current at WT P2X2 and WT P2X2/6 receptors (see transfection ratios in *parentheses*). Means ± S.E. (*error bars*) of 6–10 experiments both in this *panel* and in all further experiments are shown. The Hill coefficients for the respective WT receptors with 2-MeSATP as an agonist were as follows: P2X2, 1.8 ± 0.1; P2X2/6 (1:4 transfection), 1.2 ± 0.1. For the E_{max} and EC_{50} values as well as the exact number of experiments, see Table 1. The E_{max} and EC_{50} values as well as the Hill coefficients at the P2X2/6 receptor (1:2 transfection) were as follows: 4,327 ± 116 nA, 18.6 ± 1.4 μM, and 1.6 ± 0.2 (*Aa*). Shown are concentration-dependent changes of the slopes of the current responses from the beginning of the second s of application until its end (2-s applications in total; *Ab*). The *inset* shows the amplitude and shape of two representative scaled currents in response to 2-MeSATP (30 μM); the slopes of the current responses measured during the last 1 s of agonist application were 0.19 ± 0.06 pA/s for P2X2 and −0.27 ± 0.09 pA/s for P2X2/6. *B*, dependence of 2-MeSATP (30 μM)-induced current amplitudes on a gradual decrease of the external pH value from 7.4 to 5.4 for P2X2 and P2X2/6 receptors. Shown are representative recordings (*Ba* and *Bb*) and mean percentage changes with respect to the second current response (5-min intervals between agonist applications) at a normal pH of 7.4 (*Bc*). *, $p < 0.05$; statistically significant difference from the effect of 2-MeSATP at the P2X2 receptor. When the statistical comparison was with the predrug value of 100%, the percentage potentiation was by 33.6 ± 7% (P2X2; $p < 0.05$), 16.1 ± 11.4% (P2X2/6; transfection ratio 1:2; $p > 0.05$), and 397.2 ± 99.6% (P2X2/6; transfection ratio 1:4; $p < 0.05$). *C*, original recordings of current responses induced by increasing concentrations of 2-MeSATP at WT P2X2 (*Ca*) and WT P2X2/6 (*Cb*) receptors (indicated by *filled circles* or a *horizontal bar*). *D* and *E*, concentration-response relationships constructed for 2-MeSATP at WT and mutant (*mut*) P2X2 (*D*) or WT and mutant P2X2/6 (*E*) receptors; P2X2/6 contained either WT P2X2 and presumably non-functional mutants of P2X6 (*Ea*) or WT P2X6 and non-functional mutants of P2X2 (*Eb*). In the non-functional mutants, selected Lys and Arg residues were replaced by Ala at homologous sites also manipulated in the P2X3 subunits (Fig. 1*D*). The concentration-response relationships at the WT homomeric or heteromeric receptor are *gray*.

the respective oocyte voltage clamp measurements in supplemental Fig. 2, *Da* and *Db*).

Ca^{2+} Imaging in HEK293 Cells—In order to lend more support to our findings, we measured, in addition to the transmembrane current responses, also the $[Ca^{2+}]_i$ transients in HEK293 cells bearing P2X2, P2X3, P2X2/3, and P2X2/6 receptors. Whereas α,β-meATP (10–300 μM) caused a rapidly rising and, after its washout, also rapidly declining $[Ca^{2+}]_i$ response at homomeric P2X3 receptors (*e.g.* see Fig. 3*Ab*, *right*), similar concentrations of this agonist induced biphasic responses, slowly recovering to base line at heteromeric P2X2/3 receptors (Fig. 3*Aa*). 2-MeSATP (300 μM) at the P2X2/P2X3-K63A mutant and 2-MeSATP (10 μM) at the WT P2X2/3 receptor evoked $[Ca^{2+}]_i$ transients of practically undistinguishable shape (Fig. 3, *Aa* and *Ab*, *left*). It is noteworthy that although α,β-meATP is a selective P2X1, P2X3, P2X1/2, P2X1/5, and P2X2/3 receptor agonist without any activity at the endogenous P2Y receptors of HEK293 cells (see "Experimental Procedures"), its EC_{50} value for $[Ca^{2+}]_i$ transients in HEK293 transfected with WT P2X2/3 receptors was higher than that for transmembrane currents ($p < 0.05$; compare Figs. 1 and 3). The Hill coefficients of the two concentration-response relationships also differed from each other ($p < 0.05$). At the moment, we have no unequivocal explanation for these discrepancies. However, we tentatively suggest that Ca^{2+} influx from the extracellular space may be slightly modified by Ca^{2+}-induced Ca^{2+} release from the endoplasmic reticulum and simultaneous sequestration of $[Ca^{2+}]_i$ by its intracellular storage sites. In perfect agreement with the patch clamp investigations, Ala substitutions of the relevant AAs in the P2X3 component of the P2X2/3 receptor markedly depressed the α,β-meATP (10–300 μM)-induced current amplitudes (Fig. 3*Ba*). By contrast, replacement of the same AAs by Ala in the P2X2 component of this receptor complex had no major effect (Fig. 3*Bb*).

Because 2-MeSATP is a general P2X/P2Y receptor agonist, the amplitudes of the 2-MeSATP (0.3–300 μM)-induced $[Ca^{2+}]_i$ transients in mock-transfected HEK293 cells (mediated by endogenous P2Y receptors) were subtracted from those induced by this agonist in cells transfected with P2X2 or P2X2 plus P2X6 subunits (Fig. 3*Cb*, *left* and *right panels*; see "Experimental Procedures"). Interestingly, this time the $[Ca^{2+}]_i$ measurement yielded a lower EC_{50} value ($p < 0.05$) but identical Hill coefficient ($p > 0.05$) of the 2-MeSATP concentration-response curve as the corresponding values obtained by patch-clamp recording (compare Figs. 1 and 3), a finding that also awaits explanation.

The biphasic $[Ca^{2+}]_i$ responses appear to be typical for WT P2X2 receptors (Fig. 3*Cb*, *left*) and heteromeric receptors containing this subunit (for P2X2/6, see Fig. 3*Ca*). Again in agreement with the patch clamp investigations, Ala substitutions of the relevant AAs in the P2X6 component of the P2X2/6 receptor had no major effect on the 2-MeSATP (10–300 μM)-induced $[Ca^{2+}]_i$ transients (Fig. 3*Da*), whereas replacement of the homologous AAs in the P2X2 component of this receptor were strongly inhibitory (Fig. 3*Db*).

Two-electrode Voltage Clamp Measurements in X. laevis Oocytes—The subunit composition of the above homomeric and heteromeric receptors and their expression at the cell surface were investigated by biochemical methods in the non-mammalian *X. laevis* oocyte expression system. Therefore, it was important to prove that the functional data generated on HEK293 cells and *X. laevis* oocytes are basically identical.

In fact, in oocytes injected with cRNAs for P2X2, P2X3, and P2X6 receptor subunits, we made observations similar to those described for the mammalian cell line HEK293. Non-desensitizing current amplitudes were evoked both by α,β-meATP and 2-MeSATP (1–300 μM each) at P2X2/3 and P2X2/6 receptors, respectively (supplemental Fig. 2, *Aa* and *Ab*). When the P2X2/3 receptor complexes consisted of the P2X2 WT and P2X3 mutant subunits, the α,β-meATP (1–300 μM) current responses were greatly depressed (supplemental Fig. 2*Ca*). By contrast, the expression of the P2X3 WT subunit together with non-functional P2X2 subunits (see Fig. 2*D* and supplemental Fig. 2*B* for HEK293 cells and oocytes, respectively) only slightly displaced the α,β-meATP concentration-response curve of the WT P2X2/3 receptor to the right, indicating a moderate decrease in potency (supplemental Fig. 2*Cb*).

At P2X2/6 receptors, 2-MeSATP up to 300 μM failed to induce a notable current response at P2X2 mutant/P2X6 WT heteromers (supplemental Fig. 2*Db*), whereas the concentration-response curves of 2-MeSATP at P2X2 WT/P2X6 mutant heteromers were only modestly shifted to the left in comparison with those constructed at the WT P2X2/6 receptor (supplemental Fig. 2*Da*).

A shift of the extracellular pH from 7.4 to 5.4 depressed the E_{max} of the 2-MeSATP concentration-response curve from 34.0 ± 1.1 to 25.8 ± 0.5 μA ($n = 6$ each; $p < 0.05$) and the EC_{50} value from 4.6 ± 0.5 to 3.3 ± 0.3 μM ($p < 0.05$) but did not change its Hill coefficient significantly. Such a decrease of ATP-activated inward currents at rat P2X2/6 receptors by a decrease of the external pH from 7.5 to 5.5 was described previously (16) and appears to be valid for the oocyte expression system but not for HEK293 cells (see Fig. 2*Bc*).

Assembly and Cell Surface Trafficking of P2X2/3 and P2X2/6 Receptors—To assess the impact of the point mutations on the assembly and cell surface expression, BN-PAGE and SDS-PAGE analysis was performed. Like the homomeric wild type and mutant P2X2 receptor (data not shown) and the P2X3 receptor (30), also all of the functionally impaired heteromeric P2X2/3 mutant receptors were capable of assembling to heterotrimers and appearing at the cell surface (Fig. 4*A*, *top*). The significantly larger mass of the P2X2 protomer of 72 kDa as compared with the 55 kDa of the P2X3 protomer is reflected by a clearly detectable retarded migration of the P2X2 protomer and homotrimer in the BN-PAGE (Fig. 4, *A* and *B*, *top*) and the SDS-PAGE (Fig. 4, *A* and *B*, *bottom*) gels, respectively. As expected, the heterotrimeric assemblies of P2X2 WT and P2X3 WT or P2X3 mutant subunits migrated at a lower molecular mass than the homotrimeric P2X2 and significantly above that of the homotrimeric P2X3 receptor, clearly indicating the formation of intermediate sized heteromeric assemblies consisting of P2X2 WT and P2X3 WT or P2X3 mutant subunits (Fig. 4*A*, *top*).

A physically stable interaction between P2X2 WT and P2X3 WT or P2X3 mutant subunits is also apparent from a co-purification assay, in which we co-expressed the His-P2X2-StrepII

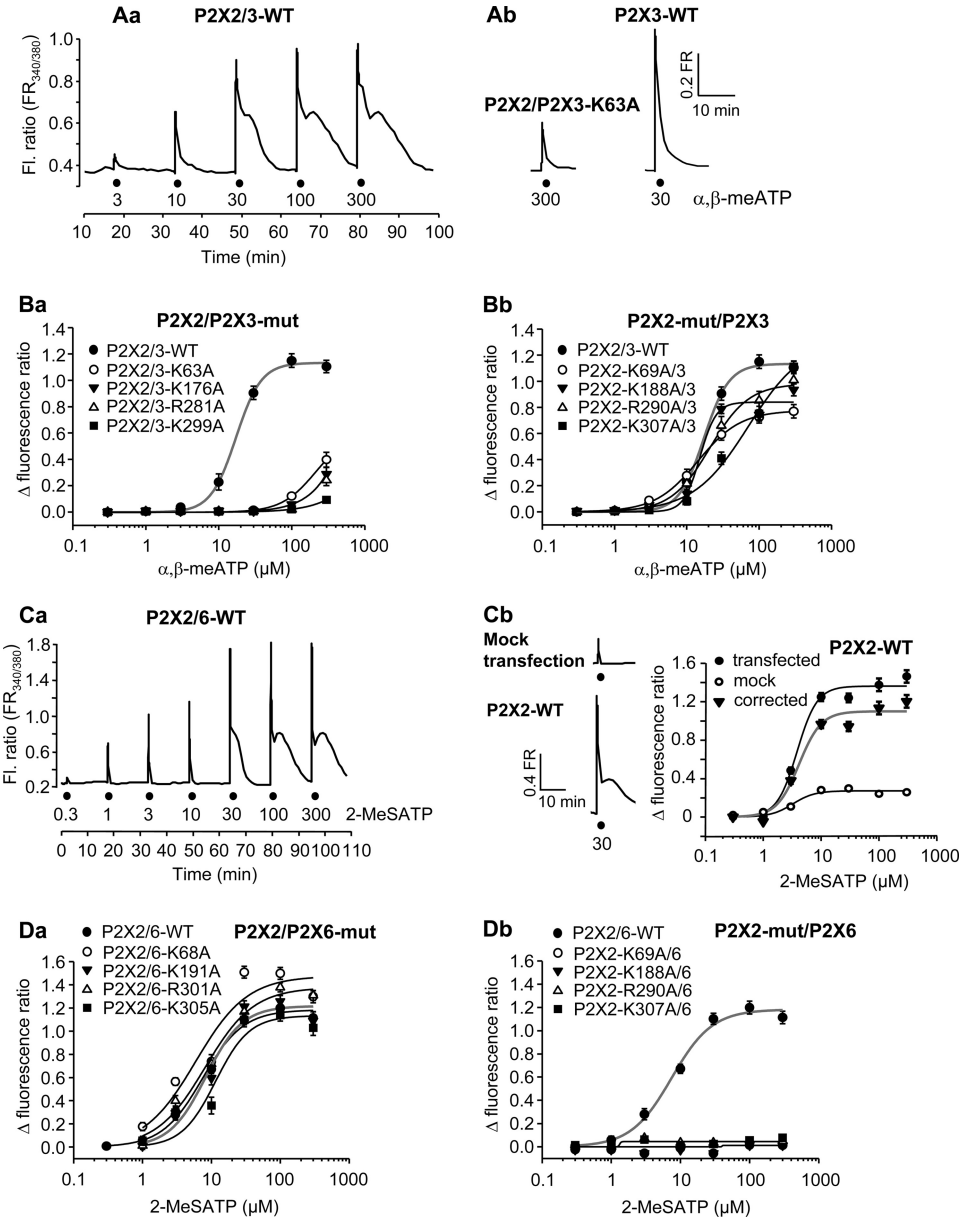

FIGURE 3. **Increase of the cytosolic free Ca^{2+} concentration ($[Ca^{2+}]_i$) by Ca^{2+} influx from the extracellular space through wt-hP2X2, hP2X6, and hP2X2/6 receptors and through the combinations of the respective WT and mutant subunits expressed in HEK293 cells.** *A*, Ca^{2+} imaging was carried out on HEK293 cells loaded by the fluorescence dye Fura-2 acetoxymethyl ester. The fluorescent ratio (*Fl. Ratio*; *FR*) provides a relative measure of $[Ca^{2+}]_i$. Increasing concentrations of 2-MeSATP (3–300 μM) were locally superfused for 5 s with 15-min intervals (as indicated by *filled circles* in the original recording shown). The shape and amplitude of the individual 2-MeSATP-induced $[Ca^{2+}]_i$ transients at WT P2X2/3 receptors (*Aa*) can be compared with the same parameters at the P2X2/P2X3-K63A mutant (*Ab*; *left*) and at the WT P2X3 receptor (*Ab*; *right*). *B*, concentration-response relationships constructed for α,β-meATP at P2X2/3 receptors containing either WT P2X2 and non-functional P2X3 subunits (*Ba*) or WT P2X3 and non-functional P2X2 subunits (*Bb*). Concentration-response curves at WT P2X2/3 receptors are also shown. *C*, original recording for a typical experiment with 2-MeSATP (0.3–300 μM) at WT P2X2/6 receptors. The shape and amplitude of the individual 2-MeSATP-induced $[Ca^{2+}]_i$ transients at WT P2X2/6 receptors (*Ca*) can be compared with the same parameters at the WT P2X2 receptor (*Cb*, *bottom left*) and in mock-transfected cells (*Cb*, *top left*). The 2-MeSATP-induced $[Ca^{2+}]_i$ transients measured in mock-transfected HEK293 cells were subtracted from the $[Ca^{2+}]_i$ transients measured in cells transfected with WT P2X2 receptors to yield the concentration-response curve of 2-MeSATP non-contaminated by the release of Ca^{2+} from intracellular pools (*Cb*, *right*). *D*, concentration-response relationships constructed for 2-MeSATP at P2X2/6 receptors, which contained either WT P2X2 and presumably non-functional mutants of P2X6 (*Da*) or WT P2X6 and non-functional mutants of P2X2 (*Db*). Concentration-response curves at WT P2X2/6 receptors are also shown. The concentration-response relationships at the WT homomeric or heteromeric receptors are *gray*. Shown are mean ± S.E. of 19–42 experiments. The E_{max} and EC_{50} values as well as the Hill coefficients of the corrected WT concentration-response curves were as follows: P2X2/3 and α,β-meATP, 1.134 ± 0.021, 17.2 ± 0.9 μM, and 2.5 ± 0.2; P2X2 and 2-MeSATP, 1.099 ± 0.072, 4.1 ± 0.9 μM, and 2.3 ± 1.0; P2X2/6 and 2-MeSATP (1:4 transfection), 1.183 ± 0.043, 7.4 ± 0.9 μM, and 1.5 ± 0.2.

(a protein bearing a C-terminal, nine-AA StrepII tag in addition to the N-terminal hexahistidine tag) as a bait together with WT or mutant His-P2X3 as the prey. Purification using metal affinity chromatography or Strep-Tactin chromatography allowed us to verify the expression of the two proteins (Fig. 4*A*, *bottom*) and to screen for the presence of co-purified His-P2X3 protein (Fig. 4*A*, *bottom*), respectively. His-P2X2-StrepII and WT or mutant His-P2X3 proteins could both be isolated by Ni^{2+}-NTA chromatography from the cells in which they were co-expressed. Purification by Strep-Tactin chromatography led to

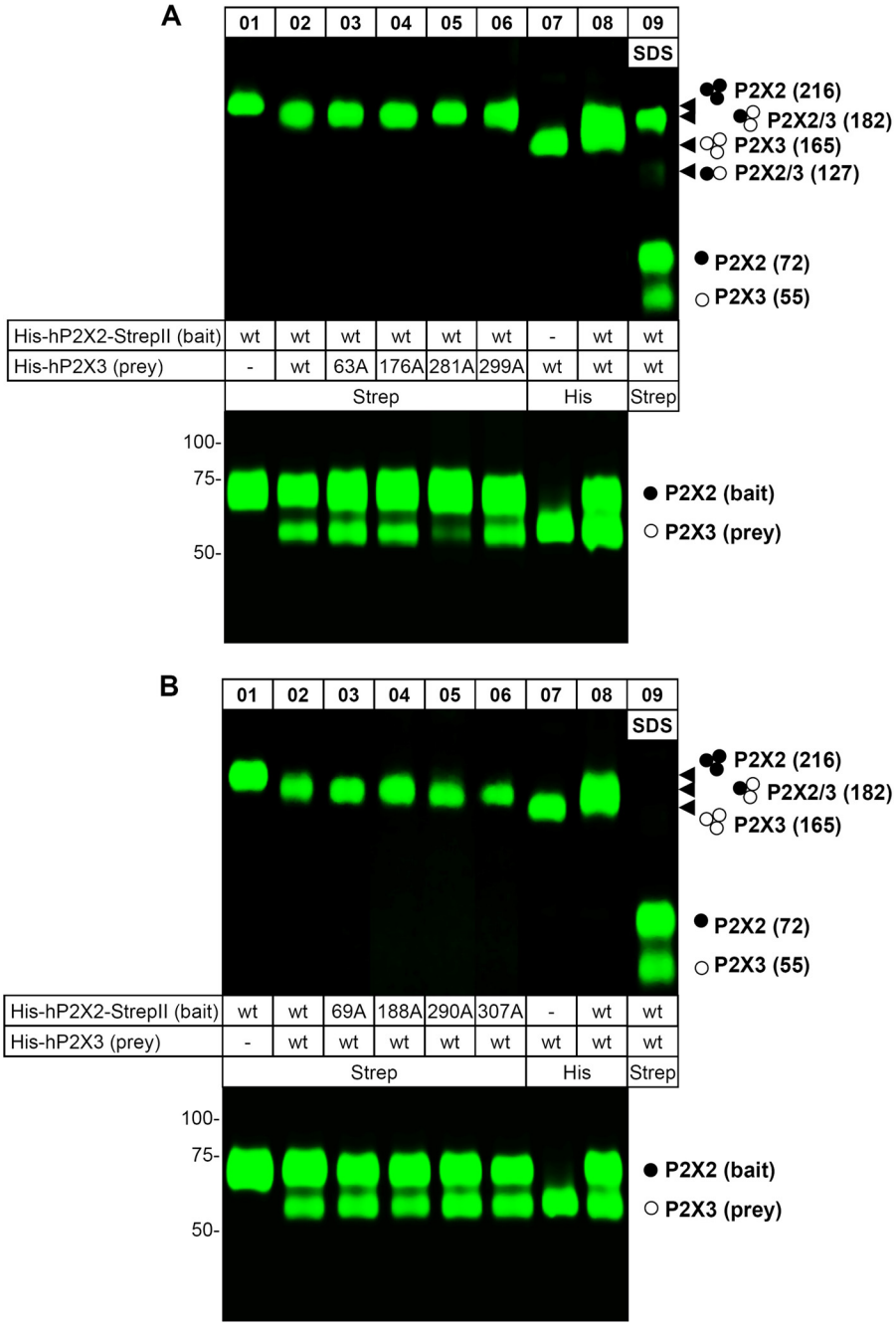

FIGURE 4. **The hP2X3 subunit co-assembles and co-purifies with the hP2X2 subunit.** The indicated proteins were purified under non-denaturing conditions from *X. laevis* oocytes by Ni^{2+}-NTA chromatography or Strep-Tactin chromatography, as indicated, resolved by BN-PAGE (*top*) or reducing SDS-PAGE (*bottom*), and visualized by Typhoon fluorescence scanning. Both the co-assembly of the WT His-hP2X2-StrepII subunit with the His-hP2X3 mutants (*A*) and the His-hP2X2-StrepII mutants with the WT His-hP2X3 subunit (*B*) are shown. The *rightmost lane* designated *SDS*, shows P2X2/3 protein migration after partial denaturation by a 1-h incubation with 0.1% SDS. The *solid* and *open circles* on the *right* indicate the numbers of hP2X2 and/or hP2X3 subunits, respectively, incorporated in the respective protein band. Migration positions of the corresponding trimeric assemblies are indicated by *arrowheads*. The *numbers* given in *parenthesis* on the *right* indicate the molecular masses calculated by referring to the SDS-PAGE-derived masses of 72 and 55 kDa for the hP2X2 and the hP2X3 protomer, respectively.

the co-isolation of the non-StrepII-tagged WT or mutant His-P2X3 proteins (Fig. 4*A*, *bottom*). When expressed alone, the His-P2X3 was not isolated (data not shown), indicating the absence of nonspecific binding of the His-P2X3 protein to the Strep-Tactin resin and thus confirming the suitability of this method for the analysis of P2X2 and P2X3 protein interaction.

Using the same biochemical techniques, we also found that the co-expression of P2X2 mutant subunits with P2X3 WT subunits resulted in the formation of heterotrimeric receptors, as judged from the characteristic migration positions in the BN-polyacrylamide gel between those of the P2X2 and P2X3 homomers (Fig. 4*B*, *top*). Also, Strep-Tactin affinity purification of co-expressed mutant His-P2X2-StrepII proteins as bait together with WT His-P2X3 as the prey led to the co-isolation of the non-StrepII-tagged WT His-P2X3 proteins (Fig. 4*B*, *bottom*).

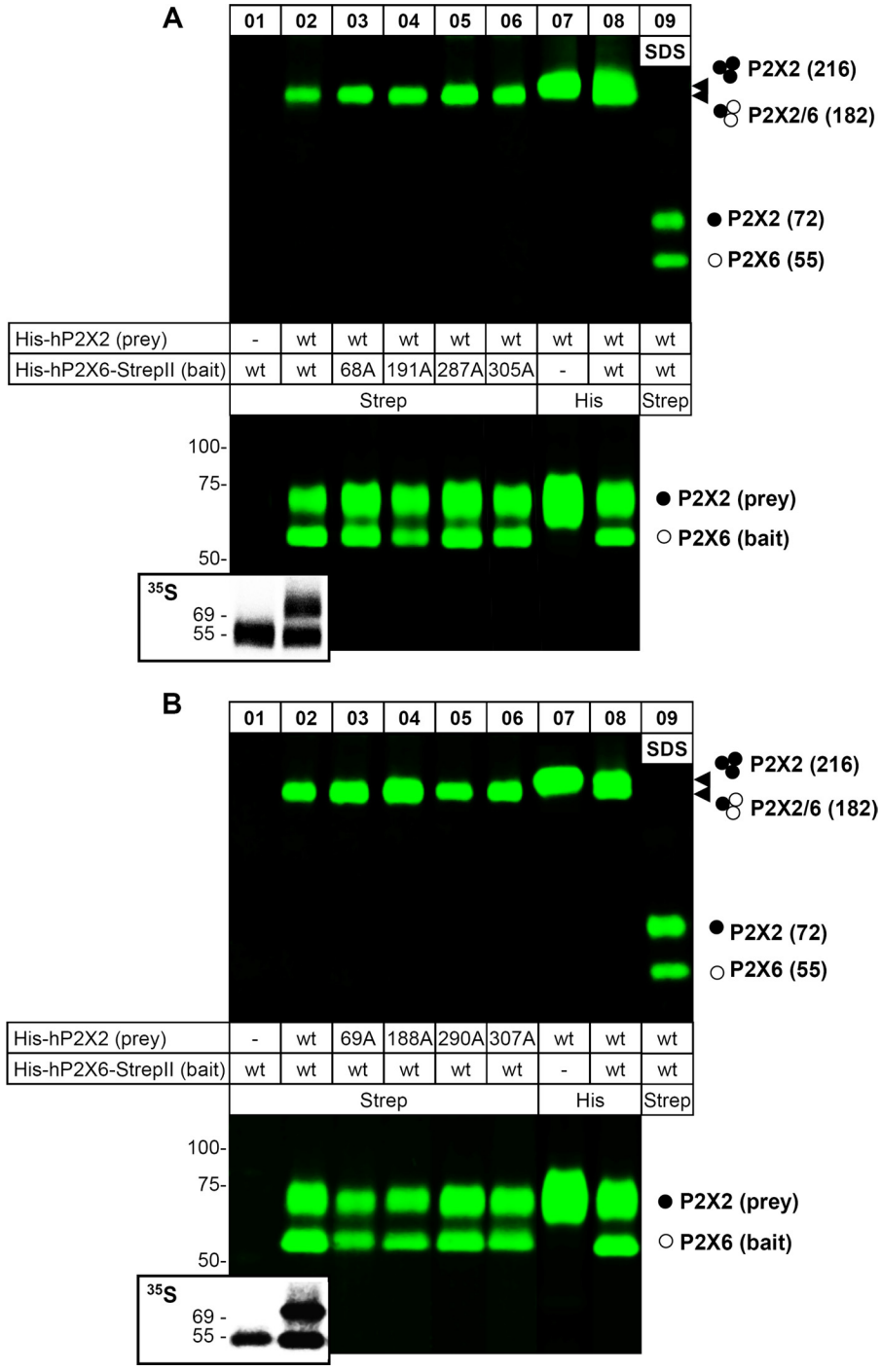

FIGURE 5. **The hP2X2 subunit coassembles and co-purifies with the hP2X6 subunit.** The indicated proteins were purified under non-denaturing conditions from *X. laevis* oocytes by Ni^{2+}-NTA chromatography or Strep-Tactin chromatography, as indicated, resolved by BN-PAGE (*top*) or reducing SDS-PAGE (*bottom*), and visualized by Typhoon fluorescence scanning. The *inset* of the *bottom panel* shows the total protein forms from corresponding lanes by [^{35}S]methionine incorporation. Both the co-assembly of the WT His-hP2X2 subunit with the His-hP2X6-StrepII mutants (*A*) and the His-hP2X2 mutants with the WT His-hP2X6-StrepII subunit (*B*) are shown. The *rightmost lane*, designated *SDS*, shows P2X2/6 protein migration after partial denaturation by a 1-h incubation with 0.1% SDS. The *solid* and *open circles* on the *right* indicate the numbers of hP2X2 and/or hP2X6 subunits, respectively, incorporated in the respective protein band. Migration positions of the corresponding trimeric assemblies are indicated by *arrowheads*. The *numbers* given in *parenthesis* on the *right* indicate the molecular masses calculated by referring to the SDS-PAGE-derived masses of 72 and 55 kDa for the hP2X2 and the hP2X6 protomer, respectively.

Oocyte-expressed heteromeric P2X2/6 receptors were also analyzed biochemically. Consistent with previous data (12), the singly expressed P2X6 subunit could be detected in the [^{35}S]methionine-labeled total form (Fig. 5, *A* and *B*, *inset* of *bottom*) but was absent at the plasma membrane (Fig. 5, *A* and *B*, *lane 1*). However, upon co-expression of the WT or a mutant His-P2X6-StrepII subunit with the WT His-P2X2 subunit, a distinct protein band was observed in the BN-polyacrylamide gel that migrated with a lower mass than that of the homomeric P2X2 receptor (Fig. 5*A*, *top*). The reduced mass of this protein

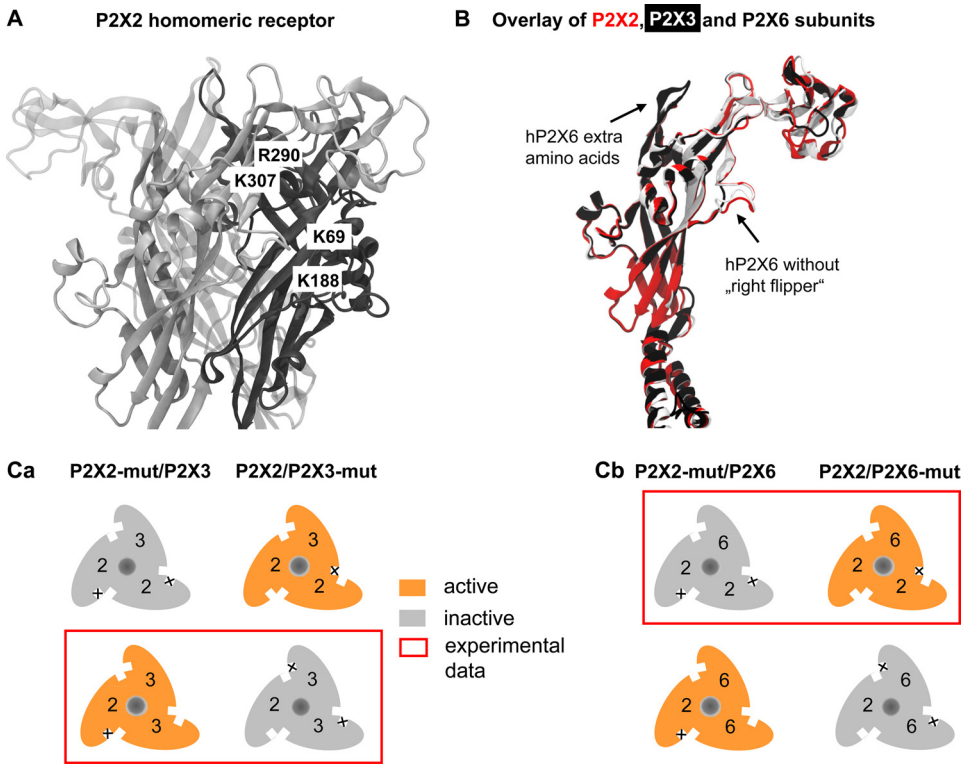

FIGURE 6. **Homology model of the P2X2 receptor and of various P2X receptor subunits; schematic representation of the subunit stoichiometry of P2X2/3 and P2X2/6 receptors.** *A*, binding-relevant Lys and Arg residues (Arg^{290}, Lys^{307}, Lys^{69}, and Lys^{188}; P2X2 numbering) of the homomeric hP2X2 receptor. Individual subunits are shown as *black*, *dark gray*, and *light gray loops*. Arg^{290} and Lys^{307} are situated at one subunit, and Lys^{69} and Lys^{188} are located at the neighboring one. The four AA residues are parts of one of the three agonist binding pouches of the P2X2 receptor. *B*, overlay of P2X2 (*red*), P2X3 (*light gray*), and P2X6 (*black*) subunits. The *right flipper* of the dolphin-like structure of these subunits is missing in P2X6. *C*, summary schematic showing the assumed subunit stoichiometry of $(P2X2)_1/(P2X3)_2$ (*Ca*) and $(P2X2)_2/(P2X6)_1$ (*Cb*). The experimental data obtained by co-expressing WT P2X2, P2X3, and P2X6 subunits and their non-functional mutants with the respective subunit partners supported the above assumption.

band can easily be reconciled with a P2X2/6 heteromer co-assembled of the larger 72-kDa P2X2 subunit and the smaller 55-kDa P2X6 subunit. The presence of the P2X6 subunit in this protein band could be demonstrated by denaturating treatment with 0.1% SDS, which led to the dissociation into two polypeptides, the larger P2X2 and the smaller P2X6 subunit (Fig. 5*A*, *lane 9*, *top*). The mass difference of these two polypeptides is also apparent from dissociation of the WT P2X2/6 trimeric protein complex in SDS-PAGE analysis (Fig. 5*A*, *bottom*).

Strep-Tactin affinity purification of co-expressed WT or mutant His-P2X6-StrepII proteins with WT His-P2X2 as the bait and the prey, respectively, led to the co-isolation of the non-StrepII-tagged WT His-P2X2 protein (Fig. 5*A*, *bottom*). Co-expression of P2X2 mutant subunits with P2X6 WT subunits resulted also in the formation of heterotrimeric receptors, as evident from the characteristic mobility shift in the BN-polyacrylamide gel toward a lower mass (Fig. 5*B*, *top*). Also, Strep-Tactin affinity purification of co-expressed WT His-P2X6-StrepII proteins with mutant His-P2X2 as bait and prey, respectively, led to the co-isolation of the non-StrepII-tagged mutant His-P2X2 proteins (Fig. 5*B*, *bottom*).

Homology Modeling of hP2X2 Receptor and of hP2X2, hP2X3, and hP2X6 Subunits; Schematic Representation of Subunit Stoichiometry of P2X2/3 and P2X2/6 Receptors—Using the published x-ray structure of the zebrafish P2X4 (31) as a template, we homology-modeled the hP2X2 receptor. The individual subunits are shown as *black*, *dark gray*, and *light gray loops*. The aromatic AA residues replaced by Ala and thereby yielding non-functional mutants are indicated in Fig. 6*A*; they are located pairwise (Arg^{290}-Lys^{306} and Lys^{69}-Lys^{188}) at two adjacent subunits and participate in the formation of a binding pocket. The overlay of the P2X2, P2X3, and P2X6 subunits shows that P2X6 does not contain the AAs forming the right flipper of the dolphin shaping all other subunits (Fig. 6*B*) (19, 31). In addition, P2X6 contains a series of extra AAs between the head and the left flipper.

A summary schematic shows our conclusions. In theory, two subunit stoichiometries are conceivable for the P2X2/P2X3 heterotrimer; 1:2 or 2:1 (Fig. 6*C*). Because our experiments indicated a loss of function only in the WT P2X2/P2X3 mutant combination (see the *framed assembly* in Fig. 6*Ca*), the 1:2 stoichiometry is compatible with the present findings. By contrast, for the P2X2/P2X6 heterotrimer, a loss of function was found only in the P2X2 mutant/WT P2X6 combination (see the *framed assembly* in Fig. 6*Cb*); therefore, in this case the combination 2:1 is compatible with the present findings.

DISCUSSION

The three-subunit composition of homomeric and heteromeric P2X receptors was originally suggested on the basis of biochemical data, including co-immunoprecipitation (6, 7) and BN-PAGE analysis as well as chemical cross-linking of subunits (12, 39). More recently, it was pointed out that co-immunopre-

cipitation may not be able to differentiate between receptor hetero-oligomers and two individual homo-oligomeric receptors closely interacting in the cell membrane (for the supposed P2X4/7 receptor, see Refs. 45 and 46). At the present time, a wealth of data supply compelling evidence for the fact that three subunits form a functional P2X receptor. Our experiments were designed to investigate the subunit composition of two neuronal heteromeric P2X receptors, composed of P2X2 and another partner (P2X3 or P2X6).

α,β-meATP activates recombinant, rapidly desensitizing P2X1 and P2X3 but not slowly desensitizing P2X2 receptors (6, 20, 34). Trinitrophenyl-ATP blocked P2X1, P2X2, and P2X2/3 receptors equally well; by contrast, diinosine pentaphosphate inhibited P2X1 receptors with a much higher affinity than P2X3 receptors (47, 48). Eventually, the selective P2X3 antagonist A-317491 exhibits comparable activities in blocking P2X2 and P2X2/3 receptors (34). Thus, P2X2/3 receptors have a ligand sensitivity resembling that of homomeric P2X3 receptors and non-desensitizing gating characteristics resembling those of homomeric P2X2 receptors (15, 49).

The situation with P2X2/6 receptors appears to be much more complex. Although co-immunoprecipitation identified P2X2 and P2X6 as possible partners for generating hetero-oligomeric complexes (10), and an oocyte expression study meticulously searched for differences between singly injected P2X2 and co-injected P2X2 and P2X6 to yield P2X2/6 (16), most differences were rather modest. It was reported that, in contrast to currents through P2X2 receptors, those through P2X2/6 receptors 1) were of smaller amplitude; 2) were sometimes biphasic and occasionally showed two phases of current decay; and 3) exhibited minor differences in their agonist and antagonist sensitivities. However, a property that unequivocally distinguished the two receptors was their opposite modulation by extracellular pH. Whereas P2X2 currents were increased after acidification of the bath solution (50), P2X2/6 currents were depressed under the same conditions (16).

It is noteworthy that only some (51) and not all groups of scientists were able to detect functional homomeric P2X6 receptors in the cell membrane (52). The reason for this discrepancy might be that P2X6 receptors either do not pass the quality check of the endoplasmic reticulum (53, 54), or if they do so, only in a partially glycosylated and non-functional form (55). Further glycosylation may result in a gain of function for some of the receptors inserted into the plasma membrane. These results perfectly agree with our own findings; homomeric P2X6 receptors failed to express at the plasma membrane of HEK293 cells.

The first part of our study confirmed and extended the observations of North and colleagues (28) by co-expressing WT P2X2 or WT P2X3 with the non-functional mutant counterparts of these subunits. In addition to the P2X3 mutants K63A and K299A situated at neighboring receptor subunits, which may interfere with binding as well as gating of the channel, because their positions are adjacent to the transmembrane segments 1 and 2 forming the channel pore, two additional mutants (K176A and R281A), being less likely to interfere with gating, were also used in the present study. We found by utilizing both HEK293 cells and oocytes as expression systems that a combination of the WT P2X2 with mutated P2X3 subunits (chosen from non-functional Ala mutants introduced in any of the four NBSs) (29) strongly inhibited or even abolished the current response to α,β-meATP, whereas the opposite combination of WT P2X3 with mutated P2X2 subunits had very little effect. Consistent with data published previously (28) these results clearly demonstrate a $(P2X2)_1/(P2X3)_2$ stoichiometry of heteromeric P2X2/3 channels, as illustrated in Fig 6*Ca*. As a correlate of the cationic fluxes induced by P2X2/3 receptor activation, $[Ca^{2+}]_i$ transients were also measured and yielded similar data. Further, we asked ourselves whether this observation might be true only when the P2X3-selective α,β-meATP is used (28), which occupies the agonist binding pouches between the P2X3/P2X3 and P2X2/P2X3 subunits but most probably not that one lying at the interface of the P2X2/P2X2 subunit (Fig. 6 *Ca*). For this purpose we applied also 2-MeSATP, which is an agonist both at homomeric P2X2 and P2X3 receptors and therefore occupies the binding sites of any of the participating receptor subunits. Thereby, it was possible to confirm that the observed phenomenon is agonist-independent.

In the second part of our study, we attempted to strengthen the hypothesis that the P2X6 subunit as a constituent of the P2X2/6 receptor complex is able to modify the original P2X characteristics, despite not being able to form a functional homomeric receptor by itself. In a mammalian cell line, the ratio of the P2X2 and P2X6 protein in P2X2/6 was either 4.1:1 or 1:2.5, depending on the ratio of the P2X2 and P2X6 plasmid cDNAs used for transfection (1:1 and 1:4) (56). However, there were no functional measurements accompanying this biochemical and atomic force microscopy investigation. We varied the plasmid cDNA ratios of the P2X2 and P2X6 subunits in the transfection reagent between 1:2 and 1:4 (the maximum ratio tested by Barrera *et al.*) (56). Indication of the formation of P2X2/6 heteromeric receptors with characteristics clearly different from those of P2X2 homomeric receptors (lower maximum current amplitude, no run-down of the current response during a 2-s application period, marked dependence of the current amplitude on the external pH) was found only at the higher transfection ratio of 1:4. A combination of the WT P2X2 subunit with P2X6 subunits mutated at sites homologous to those proven to yield non-functional P2X2 and P2X3 receptors did not alter the current response to 2-MeSATP, whereas the opposite combination of WT P2X6 with mutant P2X2 subunits resulted in non-functional receptors. Of course it cannot be excluded that at still higher transfection ratios than used by us (1:>4), P2X2/6 receptor channels with the reverse stoichiometry are formed; however, the functionality of these channels still awaits confirmation (56). In the present experiments, only P2X2/6 channels containing a minimum of two unmutated ATP binding sites were functional (Fig. 6*Cb*), as was the case also with the P2X2/3 heteromer (Fig. 6*Ca*). Therefore, a $(P2X2)_2/(P2X6)_1$ stoichiometry is the most likely one to occur.

The measurement of $[Ca^{2+}]_i$ transients caused by 2-MeSATP fully confirmed these results. In addition, our two-electrode voltage clamp data generated in *X. laevis* oocytes expressing P2X2/6 were almost identical to those obtained in the HEK293 system; the only difference was the opposite pH sensitivity of the P2X2/6 heteromer.

To exclude the possibility that the non-functional phenotype of the alanine replacement mutants within the ATP binding site originates from deficits in trimeric assembly or cell surface trafficking rather than a change in agonist action, biochemical analysis of oocytes expressing the corresponding WT and mutant P2X receptor channels was performed. Our results show that all mutants were capable of proper trimeric assembly and displayed unaltered plasma membrane trafficking. This view is further supported by the Strep-Tactin co-purification assay, which showed that all of the mutants were able to interact physically with the respective reciprocal WT subunit. Because His-P2X6-StrepII subunits reached the plasma membrane only as integral parts of the P2X2/6 heteromer (Fig. 6, *A* and *B*, *bottom*), affinity purification via the P2X6-StrepII subunit as bait (and non-Strep-tagged P2X2 as the prey) enabled us to isolate exclusively the P2X2/6 heteromer. Quantification of the relative abundance of the plasma membrane form of P2X2 and P2X6 subunits in SDS-PAGE analysis yielded a 2:1 ratio, thus also suggesting a $(P2X2)_2/(P2X6)_1$ stoichiometry.

The null hypothesis predicts that at a 1:1 protein expression ratio after transfection with two different subunits, the channel ratios for P2XA and P2XB should be 1:3:3:1 for $(P2XA)_3$, $(P2XA)_2/(P2XB)_1$, $(P2XA)_1/(P2XB)_2$, and $(P2XB)_1$; these ratios change to 1:6:12:8 and to 1:12:48:64, when the protein expression ratios are modified to 1:2 (P2X2-P2X3) and 1:4 (P2X2-P2X6), respectively. Although we did not determine the actual expression of the three receptor proteins, for P2X2/3 the subunit composition generated under the conditions of the present experiments will be by the highest likelihood $(P2X2)_1/(P2X3)_2$. Both the electrophysiological and biochemical measurements supported the existence of this preferential subunit composition in the cell membrane and its ability to respond to P2X agonists; the other possible heteromer was apparently not expressed. However, P2X2 assembled with P2X6 according to a stoichiometry of 2:1, which was not compatible with a random process of association. Nevertheless, the only subunit combination observed in the plasma membrane was $(P2X2)_2/(P2X6)_1$, which was also supported by electrophysiological measurements. Hence, recognition sites between P2X2 and its partners rather than random association may govern the subunit composition of the receptor trimers. In conclusion, P2X2 was a dominant subunit in the P2X2/6 heteromer only, and already two binding sites of the three possible ones were sufficient to allow P2X2/3 and P2X2/6 to react with their agonists (also see Refs. 32, 57, and 58).

Acknowledgments—We are most grateful to Professor Richard A. North for critically reading a previous version of the manuscript. The expert methodological support of Maria Kowalski, Nick Helms, and Gregor Pagel is gratefully acknowledged.

REFERENCES

1. Griffon, N., Büttner, C., Nicke, A., Kuhse, J., Schmalzing, G., and Betz, H. (1999) Molecular determinants of glycine receptor subunit assembly. *EMBO J.* **18,** 4711–4721
2. Klausberger, T., Sarto, I., Ehya, N., Fuchs, K., Furtmuller, R., Mayer, B., Huck, S., and Sieghart, W. (2001) Alternate use of distinct intersubunit contacts controls GABAA receptor assembly and stoichiometry. *J. Neurosci.* **21,** 9124–9133
3. Zhou, Y., Nelson, M. E., Kuryatov, A., Choi, C., Cooper, J., and Lindstrom, J. (2003) Human $\alpha4\beta2$ acetylcholine receptors formed from linked subunits. *J. Neurosci.* **23,** 9004–9015
4. Mansour, M., Nagarajan, N., Nehring, R. B., Clements, J. D., and Rosenmund, C. (2001) Heteromeric AMPA receptors assemble with a preferred subunit stoichiometry and spatial arrangement. *Neuron* **32,** 841–853
5. Schüler, T., Mesic, I., Madry, C., Bartholomäus, I., and Laube, B. (2008) Formation of NR1/NR2 and NR1/NR3 heterodimers constitutes the initial step in *N*-methyl-D-aspartate receptor assembly. *J. Biol. Chem.* **283,** 37–46
6. North, R. A. (2002) Molecular physiology of P2X receptors. *Physiol. Rev.* **82,** 1013–1067
7. Egan, T. M., Cox, J. A., and Voigt, M. M. (2004) Molecular structure of P2X receptors. *Curr. Top. Med. Chem.* **4,** 821–829
8. Roberts, J. A., Vial, C., Digby, H. R., Agboh, K. C., Wen, H., Atterbury-Thomas, A., and Evans, R. J. (2006) Molecular properties of P2X receptors. *Pflugers Arch.* **452,** 486–500
9. Köles, L., Fürst, S., and Illes, P. (2007) Purine ionotropic (P2X) receptors. *Curr. Pharm. Des.* **13,** 2368–2384
10. Torres, G. E., Egan, T. M., and Voigt, M. M. (1999) Hetero-oligomeric assembly of P2X receptor subunits. Specificities exist with regard to possible partners. *J. Biol. Chem.* **274,** 6653–6659
11. Haines, W. R., Torres, G. E., Voigt, M. M., and Egan, T. M. (1999) Properties of the novel ATP-gated ionotropic receptor composed of the P2X1 and P2X5 isoforms. *Mol. Pharmacol.* **56,** 720–727
12. Aschrafi, A., Sadtler, S., Niculescu, C., Rettinger, J., and Schmalzing, G. (2004) Trimeric architecture of homomeric P2X2 and heteromeric P2X1+2 receptor subtypes. *J. Mol. Biol.* **342,** 333–343
13. Nicke, A., Kerschensteiner, D., and Soto, F. (2005) Biochemical and functional evidence for heteromeric assembly of P2X1 and P2X4 subunits. *J. Neurochem.* **92,** 925–933
14. Torres, G. E., Haines, W. R., Egan, T. M., and Voigt, M. M. (1998) Co-expression of P2X1 and P2X5 receptor subunits reveals a novel ATP-gated ion channel. *Mol. Pharmacol.* **54,** 989–993
15. Lewis, C., Neidhart, S., Holy, C., North, R. A., Buell, G., and Surprenant, A. (1995) Coexpression of P2X2 and P2X3 receptor subunits can account for ATP-gated currents in sensory neurons. *Nature* **377,** 432–435
16. King, B. F., Townsend-Nicholson, A., Wildman, S. S., Thomas, T., Spyer, K. M., and Burnstock, G. (2000) Coexpression of rat P2X2 and P2X6 subunits in *Xenopus* oocytes. *J. Neurosci.* **20,** 4871–4877
17. Lê, K. T., Babinski, K., and Séguéla, P. (1998) Central P2X4 and P2X6 channel subunits coassemble into a novel heteromeric ATP receptor. *J. Neurosci.* **18,** 7152–7159
18. Nörenberg, W., and Illes, P. (2000) Neuronal P2X receptors. Localization and functional properties. *Naunyn Schmiedebergs Arch. Pharmacol.* **362,** 324–339
19. Browne, L. E., Jiang, L. H., and North, R. A. (2010) New structure enlivens interest in P2X receptors. *Trends Pharmacol. Sci.* **31,** 229–237
20. Coddou, C., Yan, Z., Obsil, T., Huidobro-Toro, J. P., and Stojilkovic, S. S. (2011) Activation and regulation of purinergic P2X receptor channels. *Pharmacol. Rev.* **63,** 641–683
21. Burnstock, G. (2006) Purinergic P2 receptors as targets for novel analgesics. *Pharmacol. Ther.* **110,** 433–454
22. Wirkner, K., Sperlagh, B., and Illes, P. (2007) P2X3 receptor involvement in pain states. *Mol. Neurobiol.* **36,** 165–183
23. Lalo, U., Pankratov, Y., Wichert, S. P., Rossner, M. J., North, R. A., Kirchhoff, F., and Verkhratsky, A. (2008) P2X1 and P2X5 subunits form the functional P2X receptor in mouse cortical astrocytes. *J. Neurosci.* **28,** 5473–5480
24. Palygin, O., Lalo, U., Verkhratsky, A., and Pankratov, Y. (2010) Ionotropic NMDA and P2X1/5 receptors mediate synaptically induced Ca^{2+} signaling in cortical astrocytes. *Cell Calcium* **48,** 225–231
25. Majumder, P., Trujillo, C. A., Lopes, C. G., Resende, R. R., Gomes, K. N., Yuahasi, K. K., Britto, L. R., and Ulrich, H. (2007) New insights into purinergic receptor signaling in neuronal differentiation, neuroprotection, and brain disorders. *Purinergic Signal.* **3,** 317–331
26. Schwindt, T. T., Trujillo, C. A., Negraes, P. D., Lameu, C., and Ulrich, H. (2011) Directed differentiation of neural progenitors into neurons is ac-

companied by altered expression of P2X purinergic receptors. *J. Mol. Neurosci.* **44,** 141–146
27. Jiang, L. H., Kim, M., Spelta, V., Bo, X., Surprenant, A., and North, R. A. (2003) Subunit arrangement in P2X receptors. *J. Neurosci.* **23,** 8903–8910
28. Wilkinson, W. J., Jiang, L. H., Surprenant, A., and North, R. A. (2006) Role of ectodomain lysines in the subunits of the heteromeric P2X2/3 receptor. *Mol. Pharmacol.* **70,** 1159–1163
29. Mager, P. P., Weber, A., and Illes, P. (2004) Bridging the gap between structural bioinformatics and receptor research. The membrane-embedded, ligand-gated, P2X glycoprotein receptor. *Curr. Top. Med. Chem.* **4,** 1657–1705
30. Bodnar, M., Wang, H., Riedel, T., Hintze, S., Kato, E., Fallah, G., Gröger-Arndt, H., Giniatullin, R., Grohmann, M., Hausmann, R., Schmalzing, G., Illes, P., and Rubini, P. (2011) Amino acid residues constituting the agonist binding site of the human P2X3 receptor. *J. Biol. Chem.* **286,** 2739–2749
31. Kawate, T., Michel, J. C., Birdsong, W. T., and Gouaux, E. (2009) Crystal structure of the ATP-gated P2X4 ion channel in the closed state. *Nature* **460,** 592–598
32. Sokolova, E., Skorinkin, A., Moiseev, I., Agrachev, A., Nistri, A., and Giniatullin, R. (2006) Experimental and modeling studies of desensitization of P2X3 receptors. *Mol. Pharmacol.* **70,** 373–382
33. Gerevich, Z., Zadori, Z., Müller, C., Wirkner, K., Schröder, W., Rubini, P., and Illes, P. (2007) Metabotropic P2Y receptors inhibit P2X3 receptor-channels via G protein-dependent facilitation of their desensitization. *Br. J. Pharmacol.* **151,** 226–236
34. Jarvis, M. F., and Khakh, B. S. (2009) ATP-gated P2X cation channels. *Neuropharmacology* **56,** 208–215
35. Fischer, W., Wirkner, K., Weber, M., Eberts, C., Köles, L., Reinhardt, R., Franke, H., Allgaier, C., Gillen, C., and Illes, P. (2003) Characterization of P2X3, P2Y1, and P2Y4 receptors in cultured HEK293-hP2X3 cells and their inhibition by ethanol and trichloroethanol. *J. Neurochem.* **85,** 779–790
36. von Kügelgen, I., and Harden, T. K. (2011) Molecular pharmacology, physiology, and structure of the P2Y receptors. *Adv. Pharmacol.* **61,** 373–415
37. Hausmann, R., Rettinger, J., Gerevich, Z., Meis, S., Kassack, M. U., Illes, P., Lambrecht, G., and Schmalzing, G. (2006) The suramin analog 4,4′,4″,4‴-(carbonylbis(imino-5,1,3-benzenetriylbis (carbonylimino)))tetra-kis-benzenesulfonic acid (NF110) potently blocks P2X3 receptors. Subtype selectivity is determined by location of sulfonic acid groups. *Mol. Pharmacol.* **69,** 2058–2067
38. Becker, D., Woltersdorf, R., Boldt, W., Schmitz, S., Braam, U., Schmalzing, G., and Markwardt, F. (2008) The P2X7 carboxyl tail is a regulatory module of P2X7 receptor channel activity. *J. Biol. Chem.* **283,** 25725–25734
39. Nicke, A., Bäumert, H. G., Rettinger, J., Eichele, A., Lambrecht, G., Mutschler, E., and Schmalzing, G. (1998) P2X1 and P2X3 receptors form stable trimers. A novel structural motif of ligand-gated ion channels. *EMBO J.* **17,** 3016–3028
40. Fallah, G., Romer, T., Detro-Dassen, S., Braam, U., Markwardt, F., and Schmalzing, G. (2011) TMEM16A(a)/anoctamin-1 shares a homodimeric architecture with CLC chloride channels. *Mol. Cell. Proteomics* **10,** M110.004697
41. Fiser, A., and Sali, A. (2003) Modeller. Generation and refinement of homology-based protein structure models. *Methods Enzymol.* **374,** 461–491
42. Humphrey, W., Dalke, A., and Schulten, K. (1996) VMD. Visual molecular dynamics. *J. Mol. Graph.* **14,** 33–38
43. Evans, R. J. (2010) Structural interpretation of P2X receptor mutagenesis studies on drug action. *Br. J. Pharmacol.* **161,** 961–971
44. Stojilkovic, S. S., Yan, Z., Obsil, T., and Zemkova, H. (2010) Structural insights into the function of P2X4. An ATP-gated cation channel of neuroendocrine cells. *Cell Mol. Neurobiol.* **30,** 1251–1258
45. Guo, C., Masin, M., Qureshi, O. S., and Murrell-Lagnado, R. D. (2007) Evidence for functional P2X4/P2X7 heteromeric receptors. *Mol. Pharmacol.* **72,** 1447–1456
46. Nicke, A. (2008) Homotrimeric complexes are the dominant assembly state of native P2X7 subunits. *Biochem. Biophys. Res. Commun.* **377,** 803–808
47. King, B. F., Liu, M., Pintor, J., Gualix, J., Miras-Portugal, M. T., and Burnstock, G. (1999) Diinosine pentaphosphate (IP5I) is a potent antagonist at recombinant rat P2X1 receptors. *Br. J. Pharmacol.* **128,** 981–988
48. Khakh, B. S., Burnstock, G., Kennedy, C., King, B. F., North, R. A., Séguéla, P., Voigt, M., and Humphrey, P. P. (2001) International union of pharmacology. XXIV. Current status of the nomenclature and properties of P2X receptors and their subunits. *Pharmacol. Rev.* **53,** 107–118
49. Chizh, B. A., and Illes, P. (2001) P2X receptors and nociception. *Pharmacol. Rev.* **53,** 553–568
50. King, B. F., Wildman, S. S., Ziganshina, L. E., Pintor, J., and Burnstock, G. (1997) Effects of extracellular pH on agonism and antagonism at a recombinant P2X2 receptor. *Br. J. Pharmacol.* **121,** 1445–1453
51. Collo, G., North, R. A., Kawashima, E., Merlo-Pich, E., Neidhart, S., Surprenant, A., and Buell, G. (1996) Cloning of P2X5 and P2X6 receptors and the distribution and properties of an extended family of ATP-gated ion channels. *J. Neurosci.* **16,** 2495–2507
52. Soto, F., Garcia-Guzman, M., Karschin, C., and Stühmer, W. (1996) Cloning and tissue distribution of a novel P2X receptor from rat brain. *Biochem. Biophys. Res. Commun.* **223,** 456–460
53. Barrera, N. P., Ormond, S. J., Henderson, R. M., Murrell-Lagnado, R. D., and Edwardson, J. M. (2005) Atomic force microscopy imaging demonstrates that P2X2 receptors are trimers but that P2X6 receptor subunits do not oligomerize. *J. Biol. Chem.* **280,** 10759–10765
54. Ormond, S. J., Barrera, N. P., Qureshi, O. S., Henderson, R. M., Edwardson, J. M., and Murrell-Lagnado, R. D. (2006) An uncharged region within the N terminus of the P2X6 receptor inhibits its assembly and exit from the endoplasmic reticulum. *Mol. Pharmacol.* **69,** 1692–1700
55. Jones, C. A., Vial, C., Sellers, L. A., Humphrey, P. P., Evans, R. J., and Chessell, I. P. (2004) Functional regulation of P2X6 receptors by *N*-linked glycosylation. Identification of a novel α,β-methylene ATP-sensitive phenotype. *Mol. Pharmacol.* **65,** 979–985
56. Barrera, N. P., Henderson, R. M., Murrell-Lagnado, R. D., and Edwardson, J. M. (2007) The stoichiometry of P2X2/6 receptor heteromers depends on relative subunit expression levels. *Biophys. J.* **93,** 505–512
57. Ding, S., and Sachs, F. (1999) Single channel properties of P2X2 purinoceptors. *J. Gen. Physiol* **113,** 695–720
58. Karoly, R., Mike, A., Illes, P., and Gerevich, Z. (2008) The unusual state-dependent affinity of P2X3 receptors can be explained by an allosteric two-open state model. *Mol. Pharmacol.* **73,** 224–234